

Magnetic interactions at the nanoscale in trilayer titanates $\text{LaTiO}_3/\text{SrTiO}_3/\text{YTiO}_3$

Yanwei Cao,^{1,*} Zhenzhong Yang,² M. Kareev,¹ Xiaoran Liu,¹ D. Meyers,¹ S. Middey,¹ D. Choudhury,^{1,3}
P. Shafer,⁴ Jiandong Guo,^{2,5} J. W. Freeland,⁶ E. Arenholz,⁴ Lin Gu,^{2,5} and J. Chakhalian¹

¹*Department of Physics, University of Arkansas, Fayetteville, AR 72701, USA*

²*Beijing National Laboratory for Condensed Matter Physics and Institute of Physics,
Chinese Academy of Sciences, Beijing 100190, P. R. China*

³*Department of Physics, Indian Institute of Technology, Kharagpur 721302, India*

⁴*Advanced Light Source, Lawrence Berkeley National Laboratory, Berkeley, California 94720, USA*

⁵*Collaborative Innovation Center of Quantum Matter, Beijing 100190, P. R. China*

⁶*Advanced Photon Source, Argonne National Laboratory, Argonne, Illinois 60439, USA*

(Dated: March 4, 2022)

We report on the phase diagram of competing magnetic interactions at nanoscale in engineered ultra-thin trilayer heterostructures of $\text{LaTiO}_3/\text{SrTiO}_3/\text{YTiO}_3$, in which the interfacial inversion symmetry is explicitly broken. Combined atomic layer resolved scanning transmission electron microscopy with electron energy loss spectroscopy and electrical transport have confirmed the formation of a spatially separated two-dimensional electron liquid and high density two-dimensional localized magnetic moments at the $\text{LaTiO}_3/\text{SrTiO}_3$ and $\text{SrTiO}_3/\text{YTiO}_3$ interfaces, respectively. Resonant soft X-ray linear dichroism spectroscopy has demonstrated the presence of orbital polarization of the conductive $\text{LaTiO}_3/\text{SrTiO}_3$ and localized $\text{SrTiO}_3/\text{YTiO}_3$ electrons. Our results provide a route with prospects for exploring new magnetic interfaces, designing tunable two-dimensional d -electron Kondo lattice, and potential spin Hall applications.

PACS numbers: 73.20.-r, 73.21.Cd, 75.70.-i

Magnetic interactions between the localized spins and conduction electrons are a fundamental component in the plenty of intriguing quantum many-body phenomena [1–16], a remarkable manifestation of which is the Kondo effect in heavy fermion systems [2, 7–10]. Phenomenologically, in systems with localized spins coupled to conduction electrons, the Kondo interaction [1, 9] competes with the magnetic Rudderman-Kittel-Katsuya-Yosida (RKKY) interaction [2] leading to the Doniach phase diagram [17, 18] and Kondo lattice models [2, 7, 8, 10]. In real transition metal compounds, however, the ground state strongly depends on the exchange interaction (J), electronic density ratio (n_m/n_c) of the localized magnetic moments (n_m) to conduction electrons (n_c), and the orbital character of magnetically active electrons [2, 3, 10, 13, 15]. In the strong-coupling regime with large $|J|$, the Kondo interaction prevails with the formation of a Kondo singlet state [1], whereas on the weak-coupling side (small $|J|$) depending on the value of n_m/n_c [3, 10] the RKKY interaction may give rise to either a ferromagnetic (FM) or antiferromagnetic (AFM) order between the localized spins. In particular, in the limiting case of $n_m/n_c \gg 1$, the localized spins tend to form ferromagnetic order by polarizing the conduction electrons via the Zener kinetic exchange mechanism [3, 19, 20].

In correlated d -electron heterointerfaces, besides the density ratio n_m/n_c , the dimensionality and orbital polarization of the magnetic interactions are all vital components for the formation of a ground state as exemplified by the emergent FM at the manganate-cuprates [21, 22] and manganite-ruthenate interfaces [23–26]. Moreover, it has been revealed that due to the significantly enhanced quantum fluctuations in reduced dimensions, under the scenario of Kondo state destruction [7, 27, 28] the electron and spin degrees of freedom start playing a major role to tune the heavy-fermion metal into a magnetic metal phase by crossing the quantum critical point. On the other hand, compared to f -electron heavy fermion compounds, complex oxides with partially filled d -shells are believed to be the most promising candidates for high-temperature quantum materials [7], since the d -electron *orbital* configuration intimately defines their magnetic ground states [29, 30]. To emphasize this, consider the splitting of the Ti t_{2g} band between d_{xy} - and d_{xz}/d_{yz} -subbands, which is a prime cause for the interesting emergent phenomena in the SrTiO₃-based heterostructures [31–38] including the coexistence of superconductivity and ferromagnetism [20, 39–42], the appearance of interfacial ferromagnetism [12–15, 39–46], and the formation of one-dimensional bands [14]. Since the density ratio n_m/n_c , spatial confinement, and d -electron orbital character are all important for activating novel or latent quantum states, it raises an important question: what is an experimental phase diagram for the emerging magnetic interactions at nanoscale?

To address this challenge, we synthesized a class of asymmetric trilayer superlattices (SLs) [m u.c. LaTiO₃/ n u.c. SrTiO₃/ t u.c. YTiO₃] (thereafter m LTO/ n STO/ t YTO, u.c. = unit cells; see Fig. 1). In this system, the interfacial charge-transfer was utilized to create a two-dimensional (2D) Fermi liquid interface (LTO/STO) and a spatially separated interface with localized magnetic moments (YTO/STO). This charge transfer across the layers was evidenced by combined scanning transmission electron microscopy (STEM) with electron energy loss spectroscopy (EELS) and electrical transport. Resonant soft X-ray linear dichroism (XLD) measurements were used to probe the orbital polarization of n_m and n_c electrons. The results have allowed to map out the phase diagram of competing and altered magnetic interactions at nanoscale by changing the distance between the two electronically active interfaces via the STO layer thickness n .

Trilayer SLs [3LTO/ n STO/3YTO] \times 4 ($n = 2, 3, 6$) and reference samples m LTO/ n STO ($m = 3, 20$ and $n = 2, 3, 6$) and 3YTO/ n STO ($n = 2$ and 6) were epitaxially synthesized on TbScO₃ (110) substrates by pulsed laser deposition (PLD) with a layer-by-layer mode (see details for the growth of single layer LTO, STO, and YTO films in our previous reports) [47, 48]. A JEM-ARM200F STEM, operated at 200 kV and equipped with double aberration-correctors for both probe-forming and imaging lenses, was used to perform high-angle annular-dark-field (HAADF) imaging and EELS spectroscopy. The sheet-resistances of the films were measured in van-der-Pauw geometry by Physical Properties Measurement System (PPMS, Quantum Design). XLD at Ti L_{2,3}-edge with total electron yield (TEY) mode was carried out at beamline 4.0.2 (using the vector magnet) of the Advanced Light Source (ALS, Lawrence Berkeley National Laboratory).

As shown in Fig. 1(a), in the trilayer heterostructure LTO/STO/YTO there are two inequivalent interfaces composed

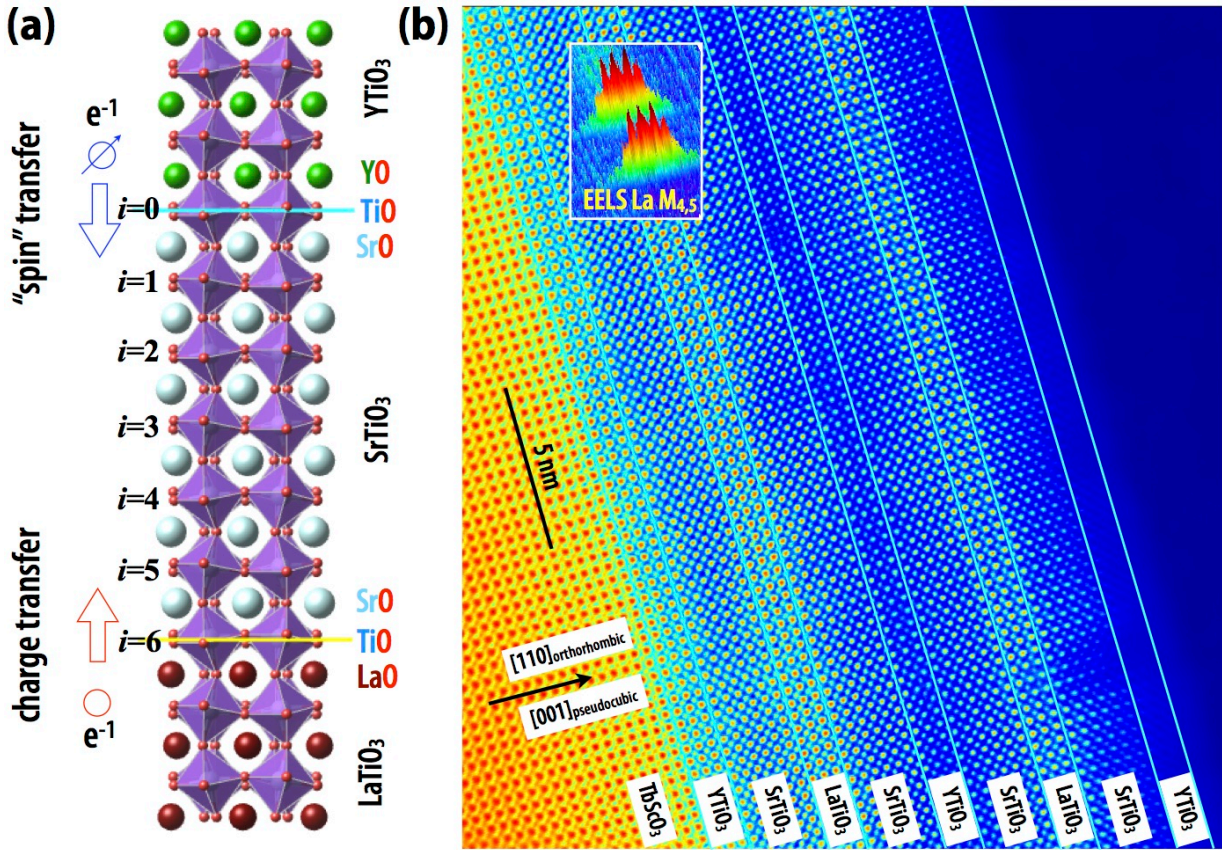


FIG. 1. (Color online) (a) Schematic view of 3LTO/6STO/3YTO with two active heterointerfaces: LTO/STO and YTO/STO. Here i denotes the i^{th} TiO_2 atomic plane of the STO layer with n unit cells. (b) HAADF-STEM image of 3LTO/6STO/3YTO. The inset is EELS spectra at La $M_{4,5}$ -edge, the three main peaks of which demonstrate the atomic sharpness of interfaces.

of two rare- and one alkaline-earth titanate compounds (LTO, YTO and STO) with a rich phase diagram [49]. In the bulk form, the Mott-insulator $\text{LaTi}^{3+}\text{O}_3$ (~ 0.2 eV gap, $\text{Ti } 3d^1$) undergoes a G-type AFM phase transition below 146 K, while the Mott-insulator $\text{YTi}^{3+}\text{O}_3$ (~ 1.2 eV gap, $\text{Ti } 3d^1$) is FM below 30 K [48, 49], and, finally, $\text{SrTi}^{4+}\text{O}_3$ remains a band-insulator (~ 3.2 eV gap, $\text{Ti } 3d^0$) over the whole temperature range. The 2D conduction electrons at the LTO/STO interface [47, 50], resulting from the charge-transfer from the LTO into STO layers (red arrow in Fig. 1(a)), serve as the Fermi sea whereas the “spin”-transfer from YTO into STO (blue arrow in Fig. 1(a)) at the other interface (YTO/STO) produces the 2D localized magnetic moments and induces spin polarization in the interface [51]. To assure that the magnetic interactions can be investigated at the unit cell scale, the interface roughness was investigated by (HAADF) STEM imaging with atomic resolution which gives the structural projection of the SLs. Taking 3LTO/6STO/3YTO as a representative example, the geometries and sequences of the trilayer layers LTO, STO and YTO in these SLs are clearly seen with atomically sharp interfaces as displayed in Fig. 1(b) and Fig. S1.

To check for the presence of the interfacial charge-transfer across the two LTO/STO and STO/YTO interfaces, the layer-resolved electronic structure of 3LTO/6STO/3YTO was investigated by atomic scale STEM-EELS line scanning across the interfaces. As seen in Fig. 2, by scanning atomic layer-resolved Ti $L_{2,3}$ -edge spectra across LTO/STO and STO/YTO interfaces (along the white-dashed line in Fig. 2(a)) with high energy (0.4 eV) and spatial (0.8 Å) resolutions, the evolution of the Ti electronic structure through the interfaces was clearly observed (Fig. 2(b)). Additionally, atomic layer-dependent lineshape and peak positions of the EELS spectra carry important information regarding the interfacial charge-transfer. Since each curve of the Ti $L_{2,3}$ -edge spectra is a convolution of both Ti^{3+} and Ti^{4+} spectra, the spectral weight of Ti^{3+} in each spectral line of $\text{Ti}^{3+}/(\text{Ti}^{3+}+\text{Ti}^{4+})$ can track and quantify the

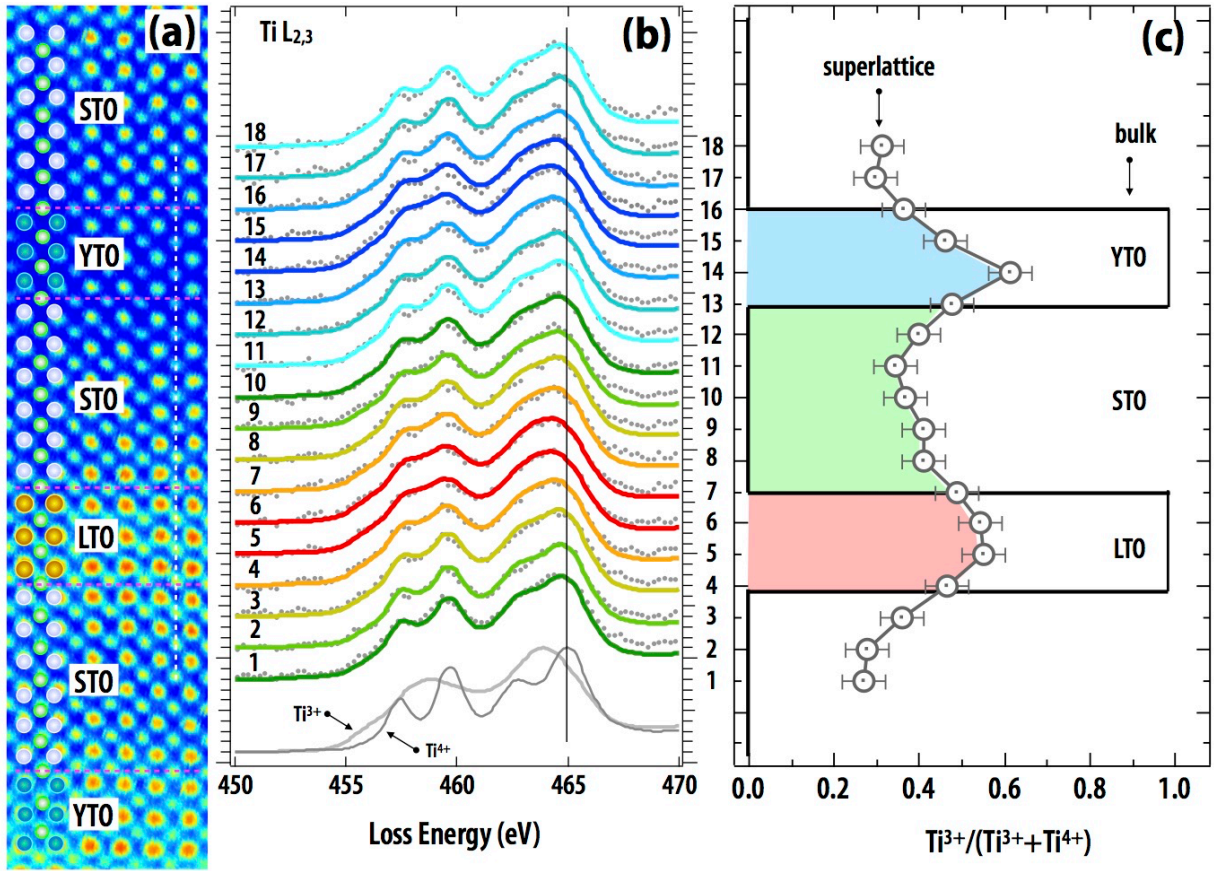


FIG. 2. (Color online). (a) HAADF image of 3LTO/6STO/3YTO. The atomic positions of the elements La (large yellow dots), Sr (large white dots), Y (large blue dots), Ti (small green dots) are labeled schematically. (b) Layer-resolved EELS spectra (scanning along the dashed white lines in (a)) with the left side of the spectra aligned to the HAADF image in (a). Reference spectra for Ti^{4+} and Ti^{3+} (acquired on bulk-like SrTiO_3 and LaTiO_3 films, respectively) at the bottom were adapted from Ref. 50. The colored solid lines are the fitting curves of layer-resolved EELS spectra to a linear combination of Ti^{4+} and Ti^{3+} spectra, whereas the experimental data are marked by small gray dots. (c) Spatial decay of the Ti^{3+} signal across the two heterointerfaces. The Ti^{3+} spectra weight is estimated from the fitting parameters of solid curves in (b).

process of interfacial charge-transfer. The direct inspection of the EELS data revealed that in addition to the the previously reported charge-transfer from LTO into STO [31, 50] there is an unexpectedly large charge-transfer from YTO into STO (see Fig. 2(c)) which leads to a localized electron layer formation at the YTO/STO interface [47, 51].

Next we investigated the properties of interfacial electrons (arising from the interfacial charge-transfer) by measuring the temperature-dependent electrical transport. As seen in Fig. 3(a) and Fig. S2[52], all three samples 3LTO/ n STO/3YTO ($n = 2, 3, 6$) show characteristic metallic behavior with a weak upturn at lower temperature. To investigate the conducting properties of the two interfaces (LTO/STO and STO/YTO) in the trilayer SLs and rule out possible contributions from defects and oxygen vacancies, *bilayer* YTO/STO and LTO/STO samples were synthesized and their transport properties were used as references (see Fig. S2); In sharp contrast to highly insulating YTO/STO [47, 51], the sheet resistances of all the LTO/STO samples (Fig. S2(a)[52]) show a 2D electron liquid (2DEL) behavior [50, 51, 53–55].

With the creation of 2D conduction electrons at LTO/STO interface, the other ingredient, that needs to be considered towards the realization of controlled magnetic interactions between two separately active heterointerfaces, is the formation of localized spins at the STO/YTO junction. As highlighted by the normalized sheet resistances in Fig. S2(d)[52] (cyan shadow area, marked as T_m) and Fig. 3(a), the other dominant feature in transport is the

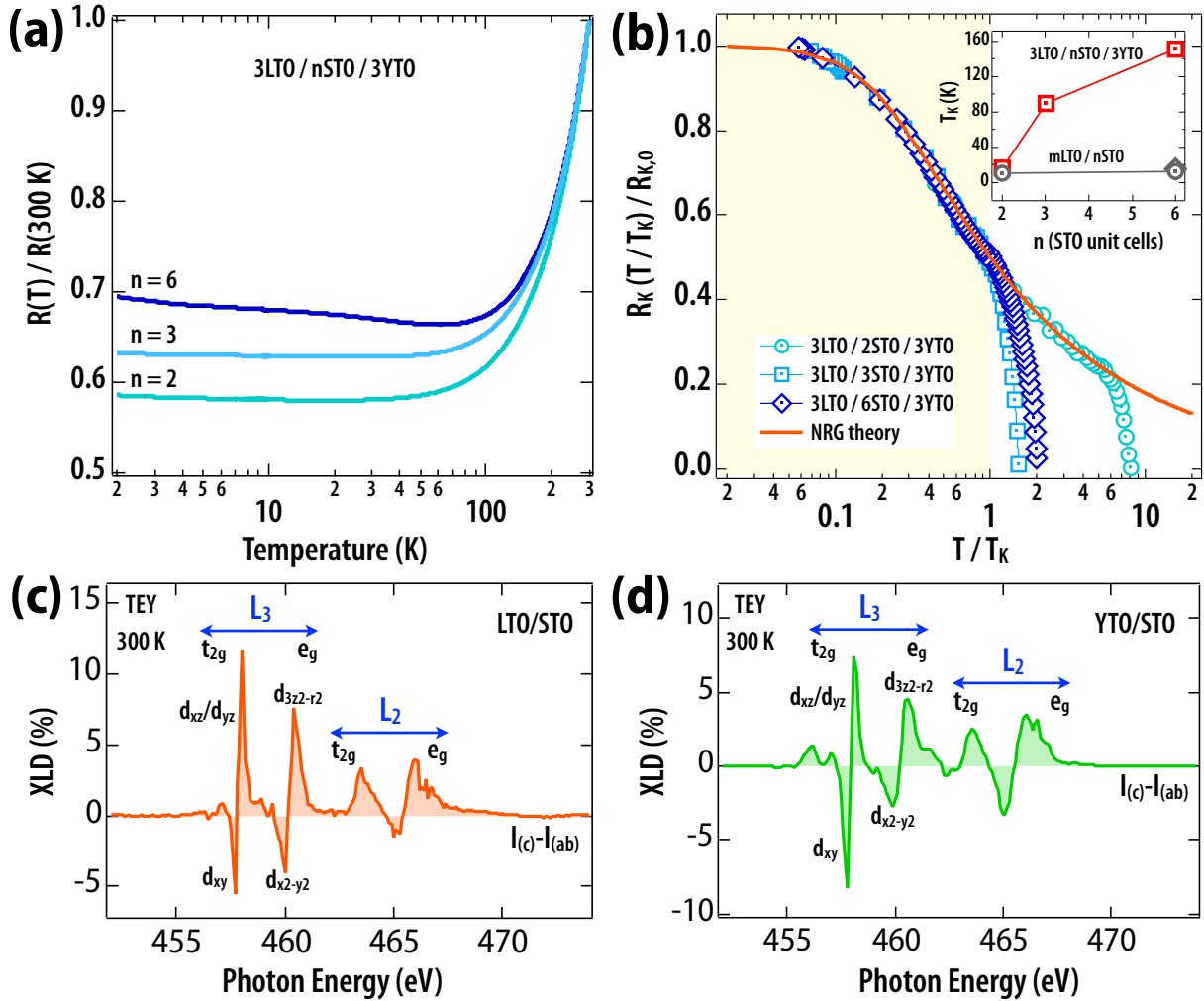


FIG. 3. (Color online). (a) Normalized sheet resistances $R(T)/R(300K)$ of 3LTO/ n STO/3YTO. (b) Experimentally and theoretically [red solid line, numerical renormalization group (NRG)] scaled Kondo resistances [$R_K(T/T_K)/R_{K,0}$] (see Eq. S4 for details). Inset, extracted n -dependent Kondo temperature T_K by fitting the experimental data of m LTO/ n STO and 3LTO/ n STO/3YTO (see Fig. S3). (c) and (d) XLD [$I(c) - I(ab)$] of 3LTO/10STO and 3YTO/2STO interfaces with surface-sensitive TEY mode, where $I(c)$ [$E \parallel c$, E is the polarization vector of the photon] is for out-of-plane and $I(ab)$ [$E \parallel ab$] is for in-plane detecting. It is noted most contribution of the signal is from top few layers (STO).

pronounced upturn of the sheet resistances at lower temperature. Previous work on titanate heterojunctions has attributed such an upturn to the Kondo effect [12, 56–59], after carefully ruling out the contributions from weak-localization [60] and electron-electron interactions [61]. One of the key features of the Kondo effect that immediately differentiates it from weak-localization and electron-electron interactions is the *universal scaling behavior* [see Fig. S3-S4 and Eq. (S1)-(S4)[52]]. As shown in Fig. 3(b), all the *trilayer* SLs obey the Kondo scaling behavior which further affirms the dominant contribution of Kondo screening to the observed upturn feature. Based on the observation that YTO/STO interface shows massive charge-transfer and yet is highly insulating, the observed Kondo behavior lends strong evidence for the formation of interfacial localized magnetic moments located on the STO side proximal to the YTO/STO interface of LTO/STO/YTO. The combined STEM/EELS and electrical transport data thus established that a 2D conduction electron layer is formed at the LTO/STO interface whereas a high-density 2D localized magnetic layer is formed in the vicinity of the STO/YTO interface (see Fig. 2 and Fig. S5).

To elucidate the link between magnetism and the d -orbital occupancy of Ti ions in the STO layer, we carried out

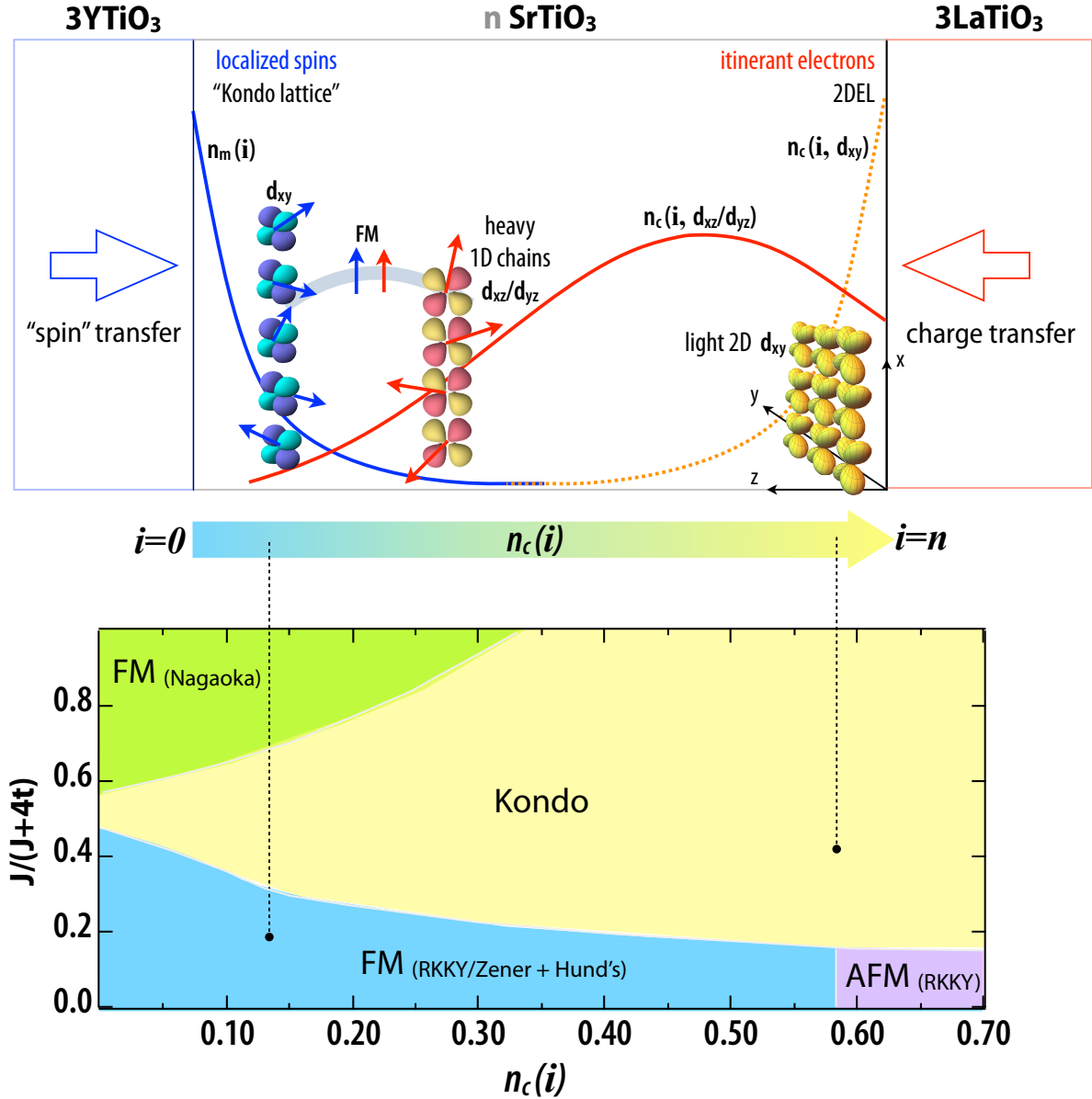


FIG. 4. (Color online) Top panel, a sketch of the TiO_2 plane (i)-dependent electronic density $[n_c(i)]$ for itinerant electrons and $n_m(i)$ for localized spins, $i \leq n$ (see Fig. 1(a)) and orbital occupancy with a charge decay away from the interfaces (see also Fig. 2(c) and Fig. S5[52]). Bottom panel, schematic phase diagram adapted from the theory [3, 10]. Near the LTO/STO interface the Kondo effect is dominant whereas ferromagnetic exchange is favored near the YTO/STO interface forming 2D d -electron Kondo lattice-like structure. Note, the phase diagram is effective for both periodic and random localized magnetic moments [3, 10]. Here, t is the electron hopping energy.

XLD measurements to probe the orbital character of both itinerant (n_c) and localized (n_m) electrons, as shown in Fig. 3(c)-(d) and Fig. S6[52]. Notice, to date the study of orbital polarization and subband splitting of interfacial Ti $3d$ band by XLD were mostly carried out on $\text{LaAlO}_3/\text{SrTiO}_3$ (LAO/STO) [62–66] and very little is known experimentally about orbital physics at the LTO/STO and, in particular, the YTO/STO interface. As shown in Fig. 3(c)-(d) and Fig. S6[52], the orbital occupancy at both LTO/STO and YTO/STO heterointerfaces exhibits a similar configuration, where the d_{xy} subband is the lowest occupied state compared to the energy position of the d_{xz}/d_{yz} subband. This orbital configuration is in a good agreement with the reported orbital physics at the LAO/STO interface [62–66].

To fully understand the magnetic interactions in LTO/STO/YTO, which strongly depend on J , n_m/n_c and orbital polarization, the STO layer thickness (n)-dependent electronic density distribution and d -orbital occupancy were investigated. As shown in Fig. S3-S5[52], from the combined EELS and transport data for both LTO/STO and YTO/STO interfaces, the presence of high-density of 2D conduction electrons ($n_c \sim 10^{14}$ - 10^{15} cm $^{-2}$ /interface) and localized moments ($n_m \sim 10^{14}$ - 10^{15} cm $^{-2}$ /interface) was deduced. To demonstrate the dependence of magnetic interactions on n_m/n_c and orbital polarization we define the i -dependent carrier densities $n_c(i)$ and $n_m(i)$, where i denotes the i^{th} TiO $_2$ atomic plane inside the STO layer counted from the YTO/STO interface (Fig. 1(a)). As seen in Fig. 2(c) and Fig. S5, based on the evolution of Ti $^{3+}/(\text{Ti}^{3+}+\text{Ti}^{4+})$ ratio, both $n_c(i)$ and $n_m(i)$ show rapid decay behavior into the STO layer.

Next we turn our attention to the orbital character of $n_c(i)$ and $n_m(i)$. Previous extensive work on STO-based heterostructures with 2DEL revealed the presence of two kinds of mobile carriers with distinct orbital dispersion, namely light d_{xy} and heavy d_{xz}/d_{yz} electrons[13, 53, 67, 68]. For the LTO/STO interface recent angle-resolved photoemission spectroscopy (ARPES) results [53] confirmed that light d_{xy} conduction electrons with large carrier density $n_c(i, d_{xy})$ are bound to the LTO/STO interface while away and deeper into the STO layer the mobile carriers are heavy electrons with d_{xz}/d_{yz} dispersion (see Fig. 4 top panel). On the other hand, for YTO/STO no experimental ARPES data are available. First principle calculations predict that the YTO/STO interface is ferromagnetic and insulating [51]. A direct comparison of the XLD lineshapes taken on Ti L $_{2,3}$ -edge for YTO/STO, LTO/STO, and LAO/STO [62–66] lends strong support to the notion that the d_{xy} band is indeed the lowest occupied state of magnetic d -electrons at the YTO/STO interface.

With the observation of $n_m(i)/n_c(i)$ and the presence of orbital polarization, it is interesting to speculate how the magnetic interactions are modulated by the STO thickness (n). We start by considering the case of a thick $n = 6$ STO layer. With a thicker STO layer, near the LTO/STO interface $n_c(d_{xy}) \gg n_m$ resulting in the formation of a Kondo singlet state, as illustrated in Fig. 4 (bottom). On the other hand, a low concentration of heavy electrons with d_{xz}/d_{yz} character disperses away from the LTO/STO interface and appears near the magnetic STO/YTO interface; upon reaching the STO/YTO interface the heavy electrons interact with the localized magnetic moments with d_{xy} character. The orbital-dependent ferromagnetic interactions then can proceed through two possible mechanisms: (i) based on the Hund's rule, the interaction between the d_{xy} and d_{xz}/d_{yz} electrons results in FM ground state [13, 15] and (ii) the Zener kinetic exchange, which may win the competition with the Kondo and RKKY interactions, again leads to the formation of a localized ferromagnetic ground state with *spin-polarized conduction electrons* [3, 10]. Based on this consideration, both the Hund's rule and Zener kinetic exchange favor the formation of localized ferromagnetism and spin-polarized conduction carriers. At the other limit when the STO layer is ultra-thin (e.g., $n = 2$), $n_c \sim n_m$ the conduction carriers lose their distinct orbital character resulting in the mixed orbital state $d_{xz}/d_{yz}/d_{xy}$. In this case the ground state is the result of a direct competition between the Kondo screening, RKKY coupling, and Hund's energy. Based on this picture, the control of STO thickness n enables the remarkable ability to modulate the critical ratio of n_c/n_m and orbital polarization to exert definitive control over the magnetic interactions.

In conclusion, we investigated the magnetic coupling between the 2D conduction electrons formed at the LTO/STO interface and the 2D localized magnetic moments at the STO/YTO interface. Due to the STO layer thickness dependent electronic density and orbital polarization of the both conduction electrons and localized spins, the competing Kondo singlet state and ferromagnetism are both present at the different TiO $_2$ planes inside the STO layer of LTO/STO/YTO. Strength of the magnetic interactions and the resulting magnetic ground state can be very effectively modulated by the thickness of STO layer with the nanoscale precision. Our findings provides an emerging magnetic phase diagram which should open prospects for exploring new magnetic interfaces [13, 15], designing tunable 2D Kondo lattices [7, 10], and potential spin Hall applications with complex oxides [11, 16, 69].

The authors deeply acknowledge numerous insightful theory discussions with Andrew Millis, Se Young Park, Gregory Fiete, and Daniel Khomskii. J. C. and D. M. were supported by the Gordon and Betty Moore Foundation EPiQS Initiative through Grant No. GBMF4534. L. Gu and J. Guo acknowledge support from National Basic Research

Program of China (Grants No. 2012CB921702 and No. 2014CB921002). X. L. was supported by the Department of Energy Grant No. DE-SC0012375 for his synchrotron work. Y. C., S. M., and M.K. were supported by the DOD-ARO under Grant No. 0402-17291. L. Gu and J. Guo acknowledge the support from the National Natural Science Foundation of China (51522212, 51421002, 11225422) and the Strategic Priority Research of the Chinese Academy of Sciences (Grant No. XDB07030200). The Advanced Light Source is supported by the Director, Office of Science, Office of Basic Energy Sciences, of the U.S. Department of Energy under Contract No. DE-AC02-05CH11231. This research used resources of the Advanced Photon Source, a U.S. Department of Energy (DOE) Office of Science User Facility operated for the DOE Office of Science by Argonne National Laboratory under Contract No. DE-AC02-06CH11357.

* yc003@uark.edu

- [1] J. Kondo, Prog. Theor. Phys. **32**, 37 (1964).
- [2] H. Tsunetsugu, M. Sigrist, and K. Ueda, Rev. Mod. Phys. **69**, 809 (1997).
- [3] T. Jungwirth, J. Sinova, J. Mašek, J. Kučera, and A. H. MacDonald, Rev. Mod. Phys. **78**, 809 (2006).
- [4] R. Yu *et al.*, Science **329**, 6 (2010).
- [5] C. Chang *et al.*, Science **340**, 167 (2013).
- [6] D. J. Kim, J. Xia, and Z. Fisk, Nat. Mater. **13**, 466 (2014).
- [7] P. Coleman, Nat. Mater. **11**, 185 (2012).
- [8] P. Coleman, *Heavy fermions: Electrons at the edge of magnetism*. (Handbook of Magnetism and Advanced Magnetic Materials, edited by H. Kronmüller and S. Parkin, Vol. 1: Fundamentals and Theory, John Wiley & Sons Ltd, 2007).
- [9] A. C. Hewson, *The Kondo Problem to Heavy Fermions* (Cambridge Univ. Press, Cambridge, 1993).
- [10] P. Fazekas and E. Müller-Hartmann, Z. Phys. B - Condensed Matter **85**, 285 (1991).
- [11] G. Y. Guo, S. Maekawa, and N. Nagaosa, Phys. Rev. Lett. **102**, 036401 (2009).
- [12] A. Brinkman *et al.*, Nat. Mater. **6**, 493 (2007).
- [13] M. Gabay and J.-M. Triscone, Nat. Phys. **9**, 610 (2013).
- [14] J. M. D. Coey, Ariando, and W. E. Pickett, MRS Bull. **38**, 1040 (2013).
- [15] J. Ruhman, A. Joshua, S. Ilani, and E. Altman, Phys. Rev. B **90**, 125123 (2014).
- [16] C. Gorini, P. Schwab, M. Dzierzawa, and R. Raimondi, Phys. Rev. B **78**, 125327 (2008).
- [17] S. Doniach, Physica B + C **91**, 231 (1977).
- [18] S. Süllo, M. C. Aronson, B. D. Rainford, and P. Haen, Phys. Rev. Lett. **82**, 2963 (1999).
- [19] C. Zener, Phys. Rev. **81**, 440 (1951).
- [20] K. Michaeli, A. C. Potter, and P. A. Lee, Phys. Rev. Lett. **108**, 117003 (2012).
- [21] J. Chakhalian *et al.*, Nat. Phys. **2**, 244 (2006).
- [22] J. Chakhalian *et al.*, Science **318**, 1114 (2007).
- [23] J. W. Freeland *et al.*, Phys. Rev. B **81**, 094414 (2010).
- [24] C. He *et al.*, Phys. Rev. Lett. **109**, 197202 (2012).
- [25] A. J. Grutter *et al.*, Phys. Rev. Lett. **115**, 047601 (2015).
- [26] P. Yordanov *et al.*, Phys. Rev. B **84**, 045108 (2011).
- [27] H. Shishido *et al.*, Science **327**, 980 (2010).
- [28] Y. Mizukami *et al.*, Nat. Phys. **7**, 849 (2011).
- [29] D. Khomskii, *Transition metal compounds* (Cambridge University press, 2014).
- [30] Y. Tokura and N. Nagaosa, Science **288**, 462 (2000).
- [31] H. Y. Hwang, Y. Iwasa, M. Kawasaki, B. Keimer, N. Nagaosa, and Y. Tokura, Nat. Mater. **11**, 103 (2012).
- [32] J. Mannhart and D. G. Schlom, Science **327**, 1607 (2010).
- [33] F. Granozio, G. Koster, and G. Rijnders, MRS Bull. **38**, 1017 (2013).
- [34] S. Stemmer and S. J. Allen, Annu. Rev. Mater. Res. **44**, 151 (2014).
- [35] J. Mannhart, D. H. A. Blank, H. Y. Hwang, A. J. Millis, and J.-M. Triscone, MRS Bull. **33**, 1027 (2008).
- [36] P. Zubko, S. Gariglio, M. Gabay, P. Ghosez, and J.-M. Triscone, Annu. Rev. Condens. Matter Phys. **2**, 141 (2011).
- [37] J. Chakhalian, A. J. Millis, and J. Rondinelli, Nat. Mater. **11**, 92 (2012).
- [38] L. Bjaalie, B. Himmetoglu, L. Weston, A. Janotti, and C. G. Van de Walle, New J. Phys. **16**, 025005 (2014).

- [39] B. Kalisky *et al.*, Nat. Commun. **3**, 922 (2012).
- [40] J. A. Bert *et al.*, Nat. Phys. **7**, 767 (2011).
- [41] L. Li, C. Richter, J. Mannhart, and R. C. Ashoori, Nat. Phys. **7**, 762 (2011).
- [42] S. Banerjee, O. Erten, and M. Randeria, Nat. Phys. **9**, 626 (2013).
- [43] J. Chakhalian, J. W. Freeland, A. J. Millis, C. Panagopoulos, and J. M. Rondinelli, Rev. Mod. Phys. **86**, 1189 (2014).
- [44] P. Moetakef *et al.*, Appl. Phys. Lett. **98**, 112110 (2011).
- [45] J. Garcia-Barriocanal *et al.*, Nat. Commun. **1**, 82 (2010).
- [46] S. Valencia *et al.*, Nat. Mater. **10**, 753 (2011).
- [47] M. Kareev *et al.*, Appl. Phys. Lett. **103**, 231605 (2013).
- [48] Y. Cao *et al.*, Appl. Phys. Lett. **107**, 112401 (2015).
- [49] M. Mochizuki and M. Imada, New J. Phys. **6**, 154 (2004).
- [50] A. Ohtomo, D. A. Muller, J. L. Grazul, and H. Y. Hwang, Nature (London) **419**, 378 (2002).
- [51] H. W. Jang *et al.*, Science **331**, 886 (2011).
- [52] Supplementary Material.
- [53] Y. J. Chang *et al.*, Phys. Rev. Lett. **111**, 126401 (2013).
- [54] J. Biscaras *et al.*, Nat. Commun. **1**, 89 (2010).
- [55] J. Biscaras *et al.*, Nat. Mater. **12**, 542 (2013).
- [56] G. M. De Luca *et al.*, Phys. Rev. B **89**, 224413 (2014).
- [57] W. Lin *et al.*, Adv. Mater. Interfaces **1**, 1300001 (2014).
- [58] S. Das *et al.*, Phys. Rev. B **90**, 081107(R) (2014).
- [59] S. Das, P. C. Joshi, A. Rastogi, Z. Hossain, and R. C. Budhani, Phys. Rev. B **90**, 075133 (2014).
- [60] Gantmakher, V. F. *Electrons and Disorder in Solids* (Oxford Univ. Press, 2005).
- [61] S. P. Chiu and J. J. Lin, Phys. Rev. B **87**, 035122 (2013).
- [62] J.-S. Lee *et al.*, Nat. Mater. **12**, 703 (2013).
- [63] M. Salluzzo *et al.*, Phys. Rev. Lett. **102**, 166804 (2009).
- [64] M. Salluzzo *et al.*, Adv. Mater. **25**, 2333 (2013).
- [65] M. Salluzzo *et al.*, Phys. Rev. Lett. **111**, 087204 (2013).
- [66] D. Pesquera *et al.*, Phys. Rev. Lett. **113**, 156802 (2014).
- [67] Z. S. Popovic and S. Satpathy, Phys. Rev. Lett. **94**, 176805 (2005).
- [68] J. H. You and J. H. Lee, Phys. Rev. B **88**, 155111 (2013).
- [69] T. Tanaka *et al.*, Phys. Rev. B **77**, 165117 (2008).

Supplementary Materials Online

Magnetic interactions at the nanoscale in trilayer titanates LaTiO₃/SrTiO₃/YTiO₃, by Cao *et al.*

The Kondo effect in 2DEL system

The upturn behavior of the sheet resistances (with saturation at ultra-low temperature) in high-quality LTO/STO and LAO/STO heterostructures has been assigned to the Kondo effect [1–5] after carefully ruling out weak localization and electron-electron interaction. In our work, the size of T_m (~ 15 K, temperature with the minimum resistance) for LTO/STO interfaces shows good agreement with the value reported by Das *et al.* [3, 4]. Generally, the Kondo temperature can be expressed by[6]

$$k_B T_K \sim D e^{-1/[2|J|\rho(E_F)]}, \quad (1)$$

$$|J| = |V|^2 \left(\frac{1}{|\epsilon_d|} + \frac{1}{|U + \epsilon_d|} \right), \quad (2)$$

where k_B is Boltzmann's constant, D is the electronic bandwidth, J for the antiferromagnetic exchange between the transferred-localized spins and conduction electrons in 2DEL, $\rho(E_F)$ is the density of states of the conduction electrons near the Fermi energy, $|V|^2$ is the hybridization parameter, U is the Coulomb repulsive energy, and ϵ_d is the binding energy of the localized spins. Under the numerical renormalization group (NRG) theory[7], it was illustrated that the electrical resistance induced by the Kondo effect (Kondo resistance) can be expressed by a universal function with only a single parameter T/T_K . The fitting quality of the Kondo resistance is usually taken as a key proof to verify the Kondo scenario[8, 9]. With the NRG theory, the function of the Kondo resistance can be obtained from experimental resistance data by[5, 10, 11]

$$R_s(T) = R_0 + aT^b + R_K(T/T_K), \quad (3)$$

$$R_K(T/T_K) = R_{K,0} \left(\frac{1}{1 + (2^{1/S} - 1)(T/T_K)^2} \right)^S, \quad (4)$$

where T_K is the Kondo temperature, R_0 is the residual resistance, the term aT^b is the general expression of transport mainly arising from electron-electron and electron-phonon contribution, $R_K(T/T_K)$ is an empirical function for the universal Kondo resistance as a function of T/T_K , $R_{K,0}$ is the Kondo sheet resistance at zero temperature, and the parameter S is fixed at 0.225 for spin $s = \frac{1}{2}$ systems. With Eq. (S3) and (S4), Figure S3 shows good agreements between the experimental data and the fitting curves with Kondo scenario for all the bilayer and trilayer samples. Furthermore, as seen in the Fig. 3b of the main text, the Kondo temperatures (T_K) and the normalized Kondo resistance ($R_K(T/T_K)/R_{K,0}$) can be extracted with the fitting parameters. On the other hand, with the limitation $T \sim 0$, the density of the localized spins leading to Kondo effect can be roughly estimated by[5]

$$R_{K,0} \approx \frac{\hbar n_{m,K}}{\pi e^2 n_s}, \quad (5)$$

where n_s and $n_{m,K}$ are the sheet concentrations of conduction electrons and localized moments, respectively. Therefore, based on the density of the conduction carriers extracted from the Hall measurements, the Kondo sheet resistances near zero temperature and the density of the localized spins can be roughly estimated with Eq. (S5), as shown in Fig. S3. Comparing with the bilayer SLs $m\text{LTO}/n\text{STO}$, the increased Kondo magnetic screening centers in trilayer SLs $3\text{LTO}/n\text{STO}/3\text{YTO}$ is consistent with the appearance of the “spin” transfer from YTO to STO.

It is important to note, the extracted values of T_K (e. g., $\sim 151\text{K}$ for $n = 6$) are far above the FM-transition temperature of $\sim 30\text{K}$ of the bulk YTO, and thus signify that these magnetic screening centers are not directly related to the bulk low temperature ferromagnetism of YTO.

Origin of the n -dependent T_K

In this part we discuss the reason why T_K can be tuned by the STO layer thickness (from $T_{K,n=2} \sim 16\text{K}$ to $T_{K,n=3} \sim 90\text{K}$, then to $T_{K,n=6} \sim 151\text{K}$, see Fig. 3b in the main text). Considering $\rho(E_F)$ is a weak decreasing function with STO thickness n (see Fig. S4(b)) in trilayer $3\text{LTO}/n\text{STO}/3\text{YTO}$ ($n = 2, 3, 6$), it is seen that $|J|$ is the main control parameter to determine T_K with the Eq. S1. Therefore, it is known naturally that $|J_{n=2}| < |J_{n=3}| < |J_{n=6}|$ with the experimental $T_{K,n=2} < T_{K,n=3} < T_{K,n=6}$. On the other hand, due to $|\epsilon_d| \ll U$ (for example, $\epsilon_d \sim -0.2\text{eV}$ for a single YO layer buried in STO and $U \sim 4\text{eV}$ is a physically reasonable value for titanates [12]), the expression of J can be simplified as $|J| \propto \frac{|V|^2}{|\epsilon_d|}$ with Eq. S2. Assuming the hybridization $|V|^2$ is a constant [13], it is derived $|J| \propto \frac{1}{|\epsilon_d|}$. Therefore, the control parameter to determine T_K can be ϵ_d . Thus, $\epsilon_{d,n=2} < \epsilon_{d,n=3} < \epsilon_{d,n=6} < E_F=0$. Such a strong (n)-dependent behavior of $\epsilon_{d,n=2,3,6}$ can be explained well by the weakened octahedra distortion with increasing STO thickness n [14]. On the other hand, with the competition among the Kondo effect, RKKY and Hund’s rule, the Kondo interaction becomes weaker when STO layer thickness is ultra-thin (e.g., $3\text{LTO}/2\text{STO}/3\text{YTO}$).

* yc003@uark.edu

References

- [1] A. Brinkman *et al.*, Magnetic effects at the interface between non-magnetic oxides. *Nat. Mater.* **6**, 493 (2007).
- [2] G. M. De Luca *et al.*, Transport properties of a quasi-two-dimensional electron system formed in $\text{LaAlO}_3/\text{EuTiO}_3/\text{SrTiO}_3$ heterostructures. *Phys. Rev. B* **89**, 224413 (2014).
- [3] S. Das *et al.*, Kondo scattering in δ -doped $\text{LaTiO}_3/\text{SrTiO}_3$ interfaces: Renormalization by spin-orbit interactions. *Phys. Rev. B* **90**, 081107(R) (2014).
- [4] S. Das, P. C. Joshi, A. Rastogi, Z. Hossain, and R. C. Budhani, Magnetothermopower of δ -doped $\text{LaTiO}_3/\text{SrTiO}_3$ interfaces in the Kondo regime. *Phys. Rev. B* **90**, 075133 (2014).
- [5] W. Lin *et al.*, Electrostatic modulation of $\text{LaAlO}_3/\text{SrTiO}_3$ interface transport in an electric double-layer transistor. *Adv. Mater. Interfaces* **1**, 1300001 (2014).
- [6] A. C. Hewson, *The Kondo Problem to Heavy Fermions* (Cambridge Univ. Press, Cambridge, 1993).
- [7] T. A. Costi, A. C. Hewson, V. Zlatic, Transport coefficient of the Anderson model via the numerical renormalization group. *J. Phys.: Condens. Matter* **6**, 2519 (1994).
- [8] W. G. van der Wiel *et al.*, The Kondo effect in the unitary limit. *Science* **289**, 2105 (2000).
- [9] J. Chen *et al.*, Tunable Kondo effect in graphene with defects. *Nat. Phys.* **7**, 535 (2011).

- [10] D. Goldhaber-Gordon *et al.*, From the Kondo regime to the mixed-valence regime in a single-electron transistor. *Phys. Rev. Lett.* **81**, 5225-5228 (1998).
- [11] M. Lee, J. R. Williams, S. Zhang, C. Frisbie, and D. Goldhaber-Gordon, Electrolyte gate-controlled Kondo effect in SrTiO₃. *Phys. Rev. Lett.* **107**, 256601 (2011).
- [12] H. W. Jang *et al.*, Metallic and insulating oxide interfaces controlled by electronic correlations. *Science* **331**, 886 (2011).
- [13] V. Yu. Irkhin and Yu. P. Irkhin, Hybridization and Kondo effect in systems with degenerate *d* and *f* shells. *J. Exp. Theor. Phys.* **80**, 334 (1995).
- [14] J. Zhang *et al.*, Correlation between metal-insulator transitions and structural distortions in high-electron-density SrTiO₃ quantum wells. *Phys. Rev. B* **89**, 075140 (2014).
- [15] J. Biscaras *et al.*, Two-dimensional superconductivity at a Mott insulator/band insulator interface LaTiO₃/SrTiO₃. *Nat. Commun.* **1**, 89 (2010).

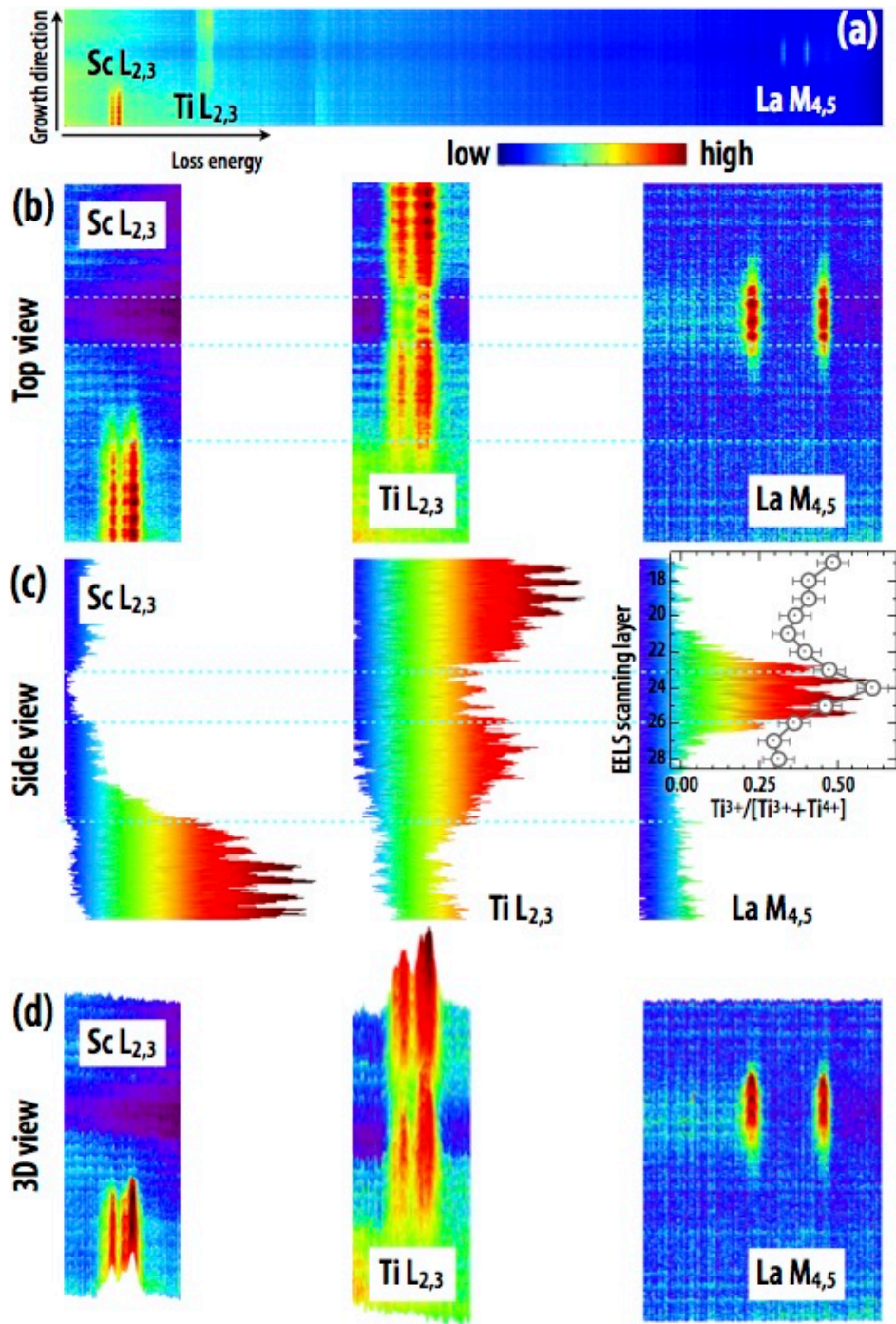


FIG. 5. (Color online) (**Figure S1**), **EELS mapping**. (a) EELS scanning along the growth direction. (b) Zoomed EELS spectra at Sc L_{2,3}-, Ti L_{2,3}-, and La M_{4,5}-edges in (a). The dashed cyan lines indicate the sharp interfaces. (c) and (d) Side and 3-dimensional view of (b), respectively. Inset in (c), spatial decay of Ti³⁺ in 3LTO/6STO/3YTO.

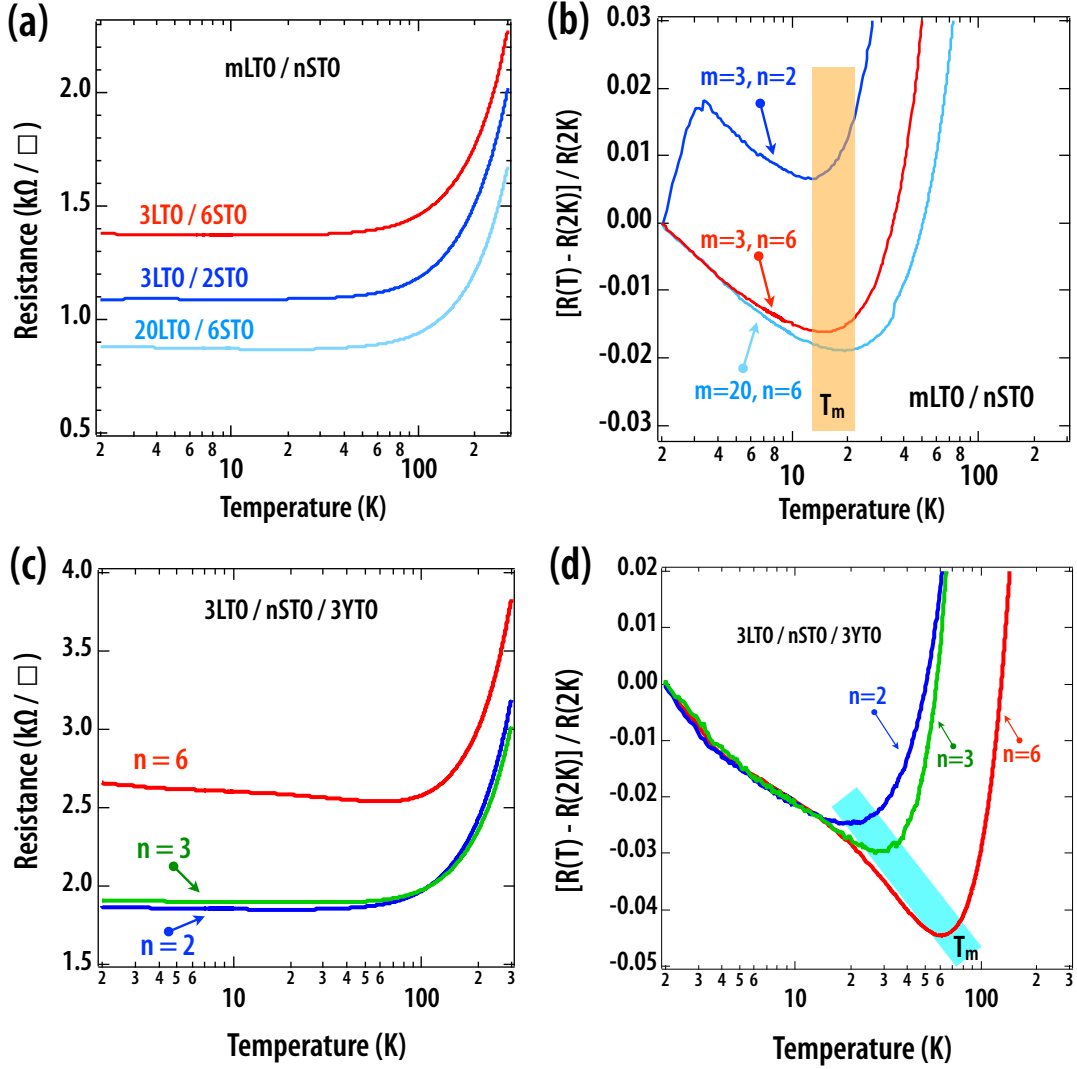


FIG. 6. (Color online) **(Figure S2), Electrical transport.** (a) Electrical sheet resistances (R) of the bicolor SLs $mLTO/nSTO$ showing a good agreement with the reported values [15]. $R = R_{total} \times I$, where R is the sheet resistance per metallic interface, R_{total} is the sheet resistance of the entire SL, and I is the number of the metallic interfaces. For example, there is 7 metallic LTO/STO interfaces in SL $[3LTO/2STO] \times 4$, thus $I = 7$. (b) Normalized sheet resistances of **a** with the sheet resistances at 2 K, $[R(T) - R(2K)]/R(2K)$. The amplitudes are zoom in $\times 9$, $\times 4$, and $\times 1$ for $3LTO/2STO$, $3LTO/6STO$, $20LTO/6STO$, respectively. The sizes of T_m (temperature with the minimum resistance) in bicolor $mLTO/nSTO$ are guided by the yellow shadow behavior, which show a nearly constant behavior. The decreased sheet resistance of $3LTO/2STO$ below 4 K may be induced by the two-dimensional superconductivity [15]. (c) Sheet resistances (R) of the trilayer SLs $3LTO/nSTO/3YTO$ ($n = 2, 3, 6$). (d) Normalized sheet resistances of (c). The amplitudes of $[R(T) - R(2K)]/R(2K)$ are $\times 2.5$, $\times 5$, and $\times 1$ for $n = 2, 3, 6$, respectively. The cyan shadow area indicates the values of T_m strongly depend on n (STO layer thickness), which varies as ~ 20 , ~ 28.5 , and ~ 61 K for $n = 2, 3, 6$, respectively. In variance to the *bicolor* LTO/STO reference samples with T_m nearly independent of the thickness of individual STO (n) or LTO (m) layers, the presence of YTO in the LTO/ n STO/YTO SLs gives rise to a sharp and systematic increase in T_m with the STO layer thickness, n .

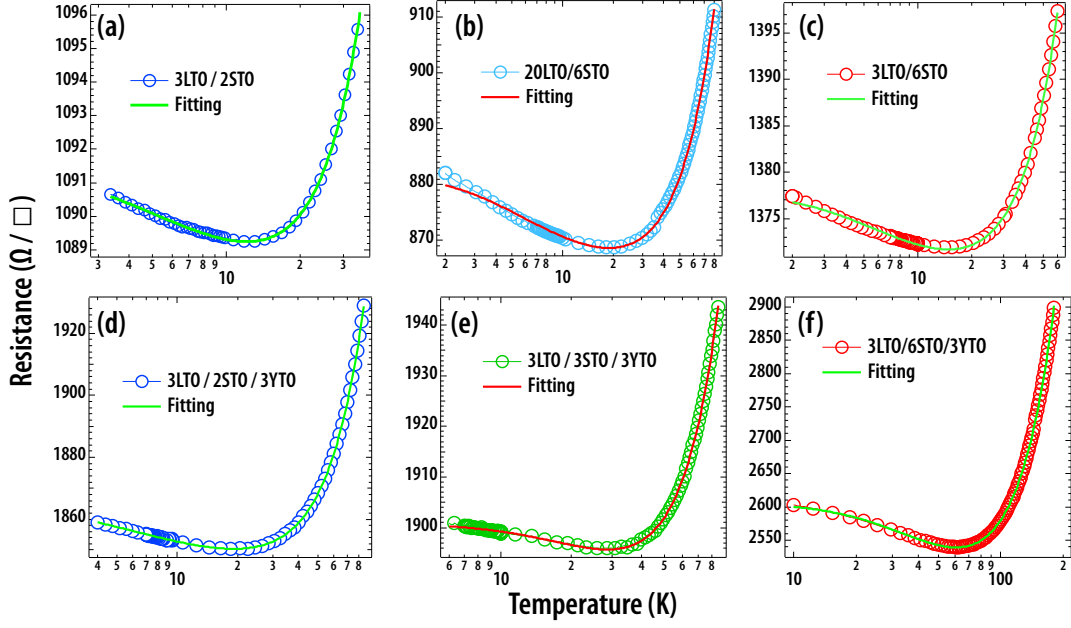


FIG. 7. (Color online) **(Figure S3), Fitting of the sheet resistances with the Kondo effect scenario.** (a)-(f) Comparison of the fitting curves (solid lines, using Eq. S3-S4) with experimental data (circles). (a)-(c), bilayer SLs m LTO/ n STO ($m = 3, n = 2; m = 20, n = 6$ and $m = 3, n = 6$, respectively). (d)-(f), trilayer SLs 3LTO/ n STO/3YTO ($n = 2, 3, 6$).

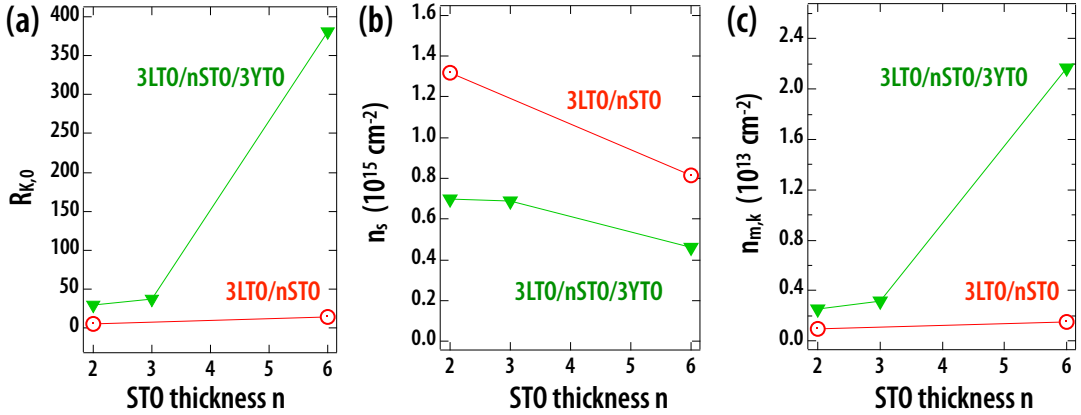


FIG. 8. (Color online) **(Figure S4), Density of conduction electrons and Kondo localized spins.** (a) Kondo resistance near zero temperature extracted from Fig. S3. (b) Carrier density per interface for bilayer and trilayer SLs measured from Hall resistances at 10 K. (c) Density of the magnetic scattering centers estimated with Eq. S5.

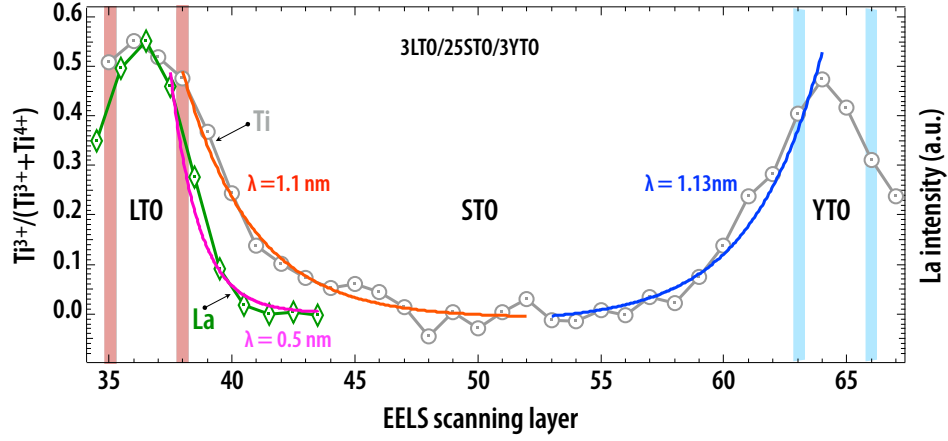


FIG. 9. (Color online) (Figure S5), **Spatial decay of Ti^{3+} and La in 3LTO/25STO/3YTO**. The regular charge-transfer was observed from LTO to STO resulting in 2DEL, while the special “spin” transfer was uncovered from YTO to STO leading to the localized spins. The tails of the charge spatial decay can be fitted well by a exponential function decay (solid red and pink lines) $e^{-z/\lambda}$ for the two interfaces, where z is the number of the TiO_2 -plane or the LaO -plane and λ is the electron decay length.

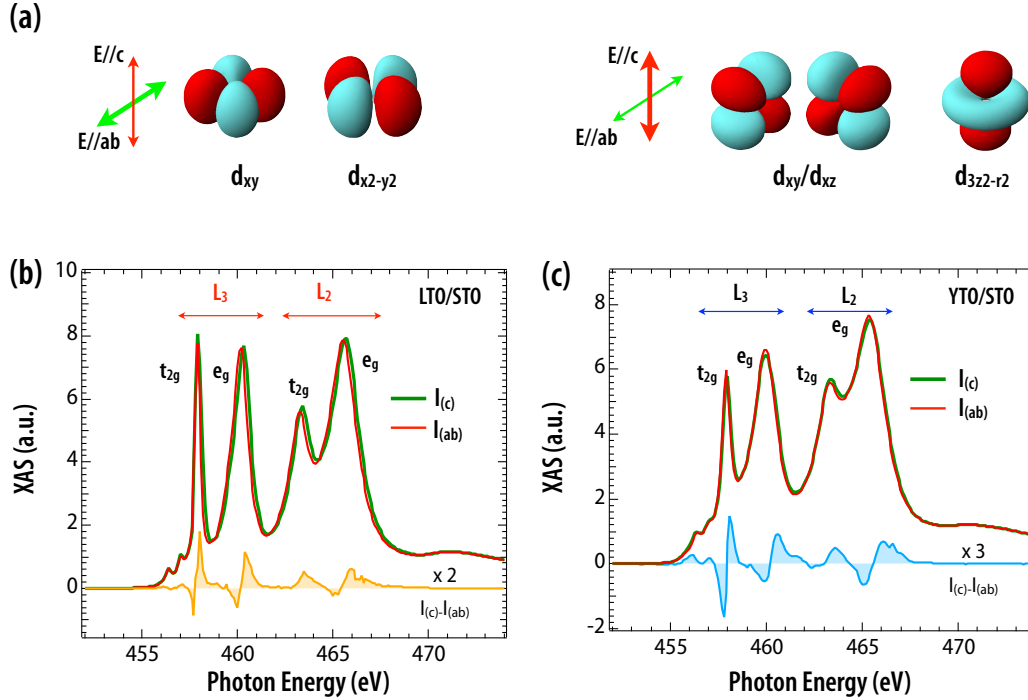


FIG. 10. (Color online) (Figure S6), **Linearly-polarized X-ray absorption spectra**. (a) Schematic of linear polarization vector of the photon E and orbital characters. Out-of-plane [$I(c)$, $E \parallel c$ and E is the linear polarization vector of the photon] and in-plane [$I(ab)$, $E \parallel ab$] linearly polarized X-ray were used to measure XAS of SLs 3LTO/10STO and 3YTO/2STO at Ti $L_{2,3}$ -edge with total electron yield (TEY, surface sensitive) mode at room temperature. The contribution of linearly polarized XAS signal on Ti $L_{2,3}$ -edge for t_{2g} (or e_g) band arises mainly from the unoccupied Ti d_{xy} (or $d_{x^2-y^2}$) [in-plane $I(ab)$] and d_{xz}/d_{yz} (or $d_{3z^2-r^2}$) [out-of-plane $I(c)$] states. It is noted STO is the cap layer for these two samples which guarantees the most contribution of XLD signal is from the STO layer. (b) LTO/STO superlattice. (c) YTO/STO superlattice.